Multistep Oxidation of Diethynyl Oligophenylamine-Bridged Diruthenium and Diiron Complexes

Jing Zhang,[†] Shen-Zhen Guo,[†] Yu-Bao Dong,[†] Li Rao,[†] Jun Yin,[†] Guang-Ao Yu,[†] František Hartl,*[,‡] Sheng Hua Liu*[,†]

[†] *Key Laboratory of Pesticide and Chemical Biology, Ministry of Education, College of Chemistry, Central China Normal University, Wuhan 430079, P.R. China*

[‡] *Department of Chemistry, University of Reading, Whiteknights, Reading RG6 6AD, U.K.*

Crystallographic Information

Table S1. Crystal data and parameters of data collection and refinement for complexes **1a** and **2a**.

Complex	**1a**	**2a**
Formula	$C_{94}H_{91}NP_4Ru_2$	$C_{106}H_{100}N_2P_4Ru_2 \cdot 3(CH_2Cl_2)$
Formula weight	1560.70	1982.67
Temperature (K)	298(2)	296(2)
Crystal system	Monoclinic	Triclinic
Space group	*C*2/*c*	*P*-1
a (Å)	42.877(6)	9.848 (3)
b(Å)	9.6957(14)	14.954 (5)
c(Å)	21.349(3)	16.443 (6)
α (°)	90	77.951 (5)
β (°)	112.940 (2)	89.872 (5)
γ (°)	90	80.650 (5)
V (Å^3)	8173 (2)	2335.4 (14)
Z	4	1
Density (calculated) (Mg/m^3)	1.268	1.410
Absorption coefficient (mm^{-1})	0.49	0.61
F(000)	3240	1024
Crystal size (mm^3)	0.20 × 0.20 × 0.10	0.20 × 0.20 × 0.20
Theta range for data collection (°)	1.03 to 28.00	1.267 to 28.128

Index ranges	-56≤*h*≤55, -12≤*k*≤12, -27≤*l*≤28	-13≤*h*≤13, -19≤*k*≤19, -21≤*l*≤21
Reflections collected	34815	19652
Independent reflections	9817 [*R*(int) = 0.037]	10847 [*R*(int) = 0.053]
Max. and min. transmission	0.952 and 0.908	0.746 and 0.539
Data / restraints / parameters	9817 / 0 / 462	10847 / 39 / 582
Goodness-of-fit on F^2	1.132	1.081
Final *R* indices [$I>2\sigma(I)$]	*R*1 = 0.0450, w*R*2 = 0.1188	*R*1 = 0.1398, w*R*2 = 0.4261
R indices (all data)	*R*1 = 0.0664, w*R*2 = 0.1389	*R*1 = 0.1608, w*R*2 = 0.4097
Largest diff. peak and hole	1.09 and -0.37 e.$^{-3}$	5.85 and -1.63 e.$^{-3}$

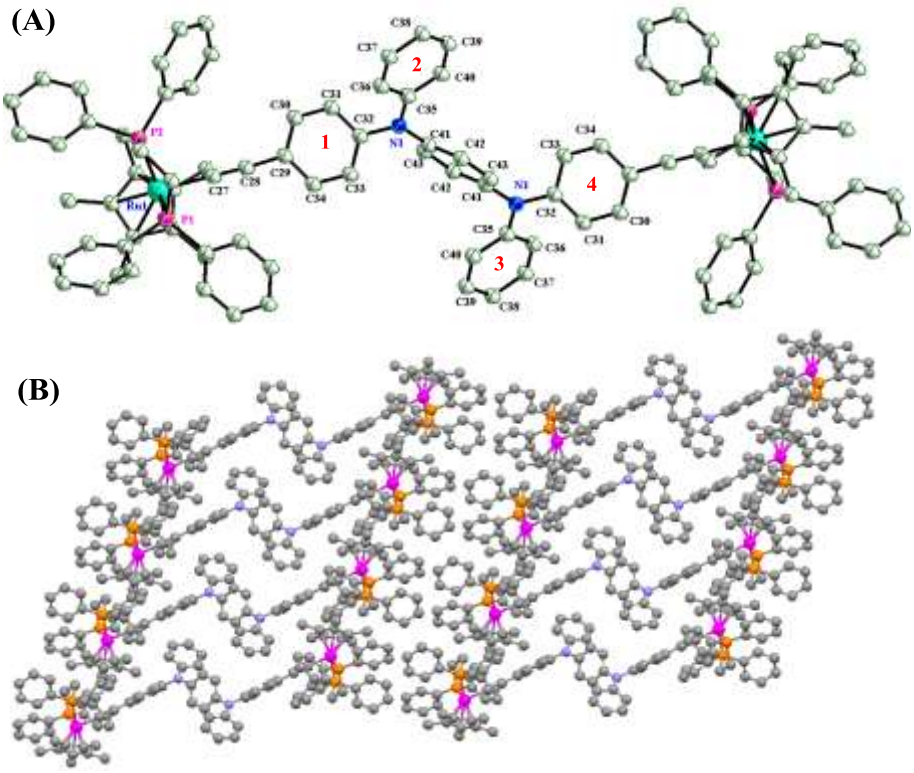

Figure S1. X-ray crystal structure of **2a** shown with thermal ellipsoids at the 50% probability level (A), and the packing view of **2a** (B). Hydrogen atoms and co-crystallized solvent molecules have been omitted for clarity. CCDC 1435473.

Spectro-Electrochemical Information

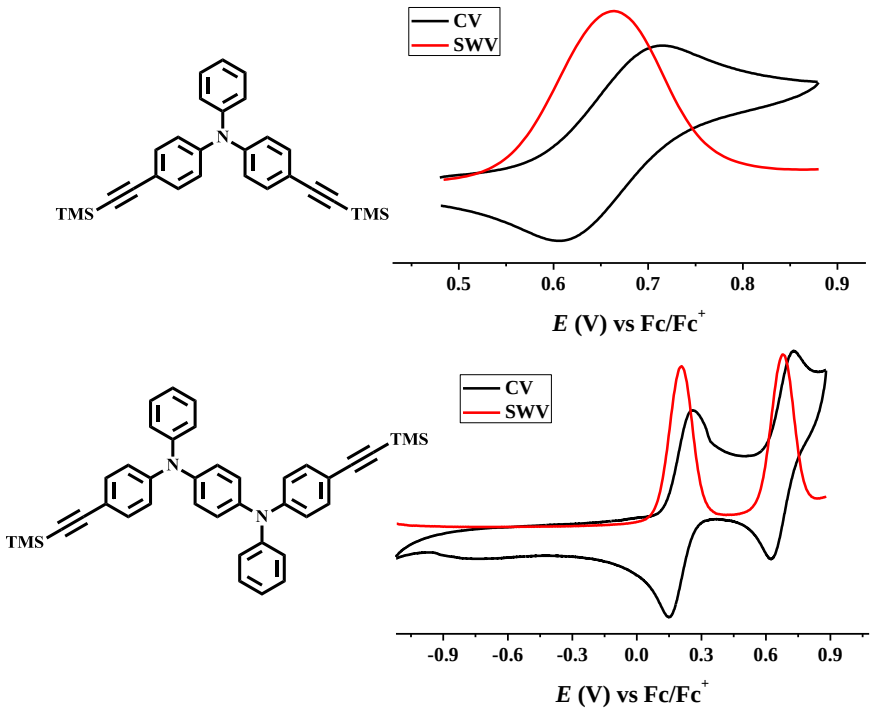

Figure S2. Cyclic voltammograms (CV, v = 50 mV s^{-1}) and corresponding square-wave voltammograms (SWV, at f = 10 Hz and t_p = 25 mV) of the ligand bridge precursors **1d** (top) and **2d** (bottom).

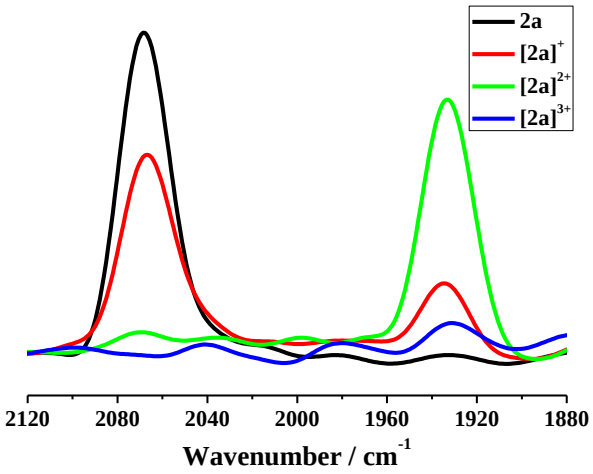

Figure S3. IR spectra in the ν(C≡C) region recorded for complex **2a** in four different oxidation states generated in $CH_2Cl_2/10^{-1}$ M n-Bu_4NPF_6 at 298 K within an OTTLE cell. Note that singly oxidized [**2a**]$^+$ cannot be obtained in the pure form due to its partial valence disproportionation to **2a** and [**2a**]$^{2+}$.

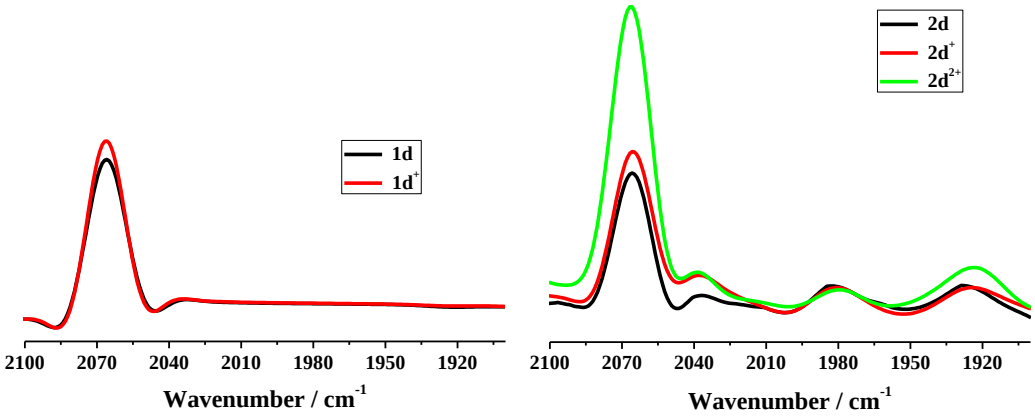

Figure S4. IR spectra recorded in the *ν*(C≡C) region for compounds **1d** and **2d** in different oxidation states (0, +1 or +2) generated in $CH_2Cl_2/10^{-1}$ M *n*-Bu_4NPF_6 at 298 K within an OTTLE cell.

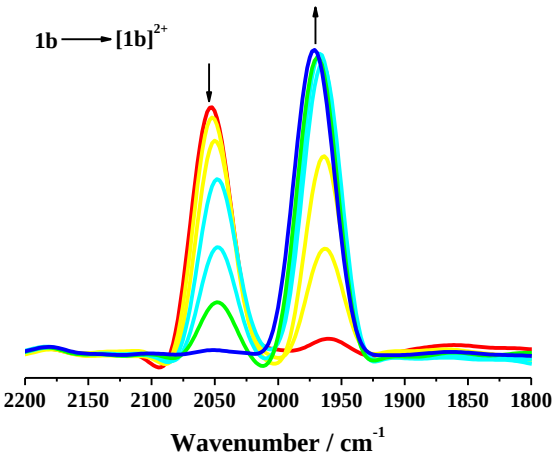

Figure S5. IR spectra recorded in the *ν*(C≡C) region during the electrochemical oxidation of **1b** into $[\mathbf{1b}]^{2+}$ in $CH_2Cl_2/10^{-1}$ M *n*-Bu_4NPF_6 at 298 K within an OTTLE cell. The process involves an equilibrium with the minor mixed-valence state $[\mathbf{1b}]^{+}$ (see also Figure S6).

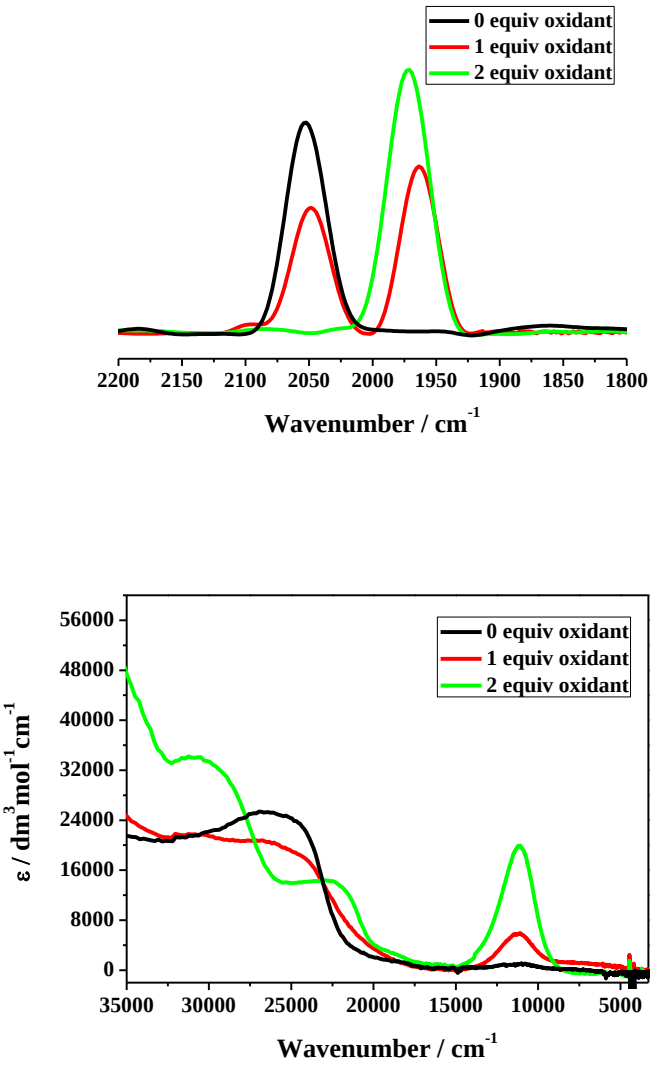

Figure S6. Infra-red (top) and electronic absorption (bottom) spectra of parent complex **1b** (black) and [**1b**]$^{2+}$ (green) recorded after oxidation of **1b** with ferrocenium hexafluorophosphate ($FcPF_6$) in CH_2Cl_2 at room temperature. The intermediate spectra (red) correspond to the oxidation with 1 equiv. $FcPF_6$, which produced some [**1b**]$^{+}$ identified by the transient NIR absorption below 10000 cm^{-1}.

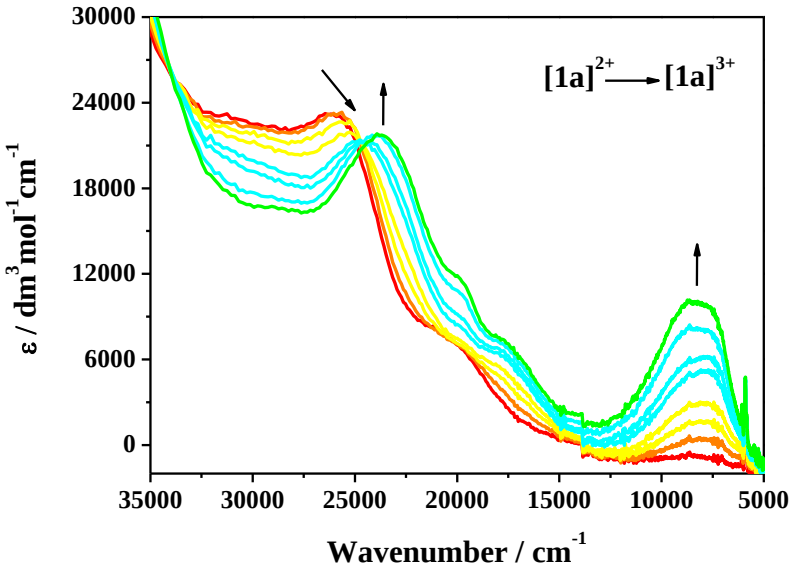

Figure S7. UV-vis-NIR spectral changes recorded during the oxidation of complex [**1a**]$^{2+}$ to [**1a**]$^{3+}$ in $CH_2Cl_2/10^{-1}$ M *n*-Bu_4NPF_6 at 298 K within an OTTLE cell.

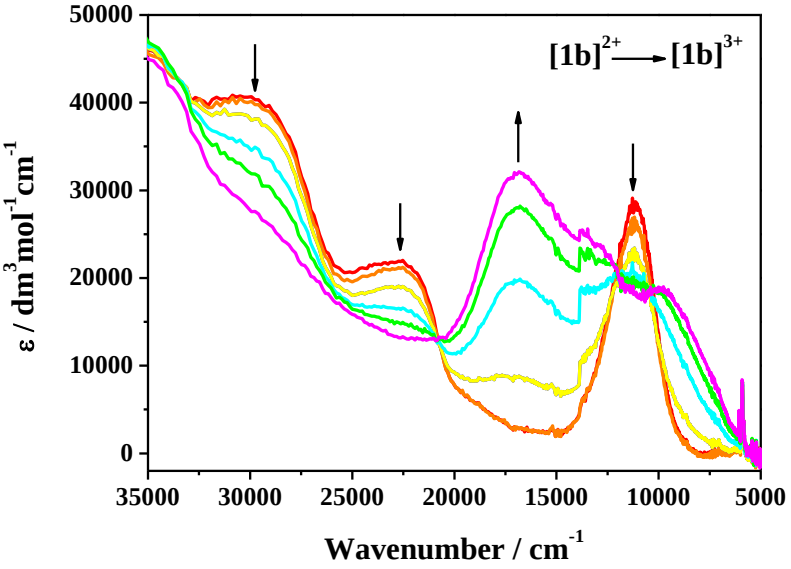

Figure S8. UV-vis-NIR spectral changes recorded during the oxidation of complex [**1b**]$^{2+}$ to [**1b**]$^{3+}$ in $CH_2Cl_2/10^{-1}$ M *n*-Bu_4NPF_6 at 298 K within an OTTLE cell.

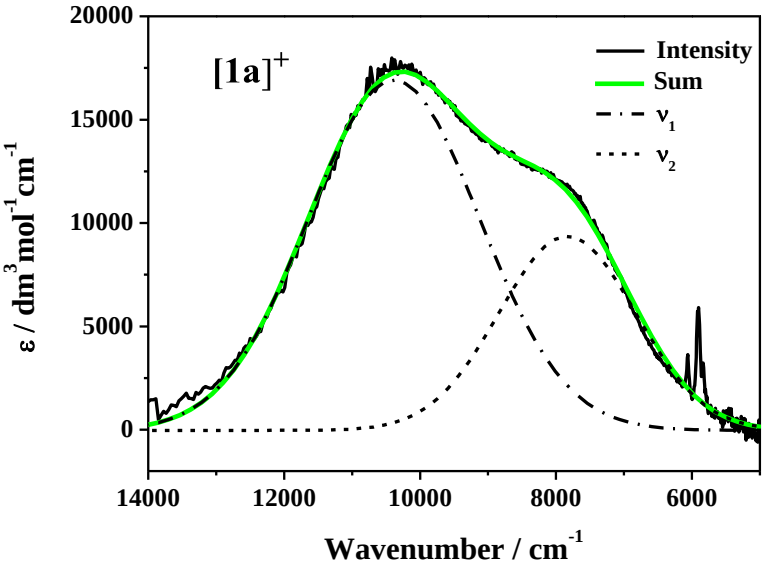

Figure S9. Deconvolution of the intense NIR absorption of [**1a**]$^{+}$ (recorded during the anodic spectroelectrochemistry, see Figure 4 in the main text) into two Gaussian-shaped bands. Table S2 presents the corresponding electronic parameters.

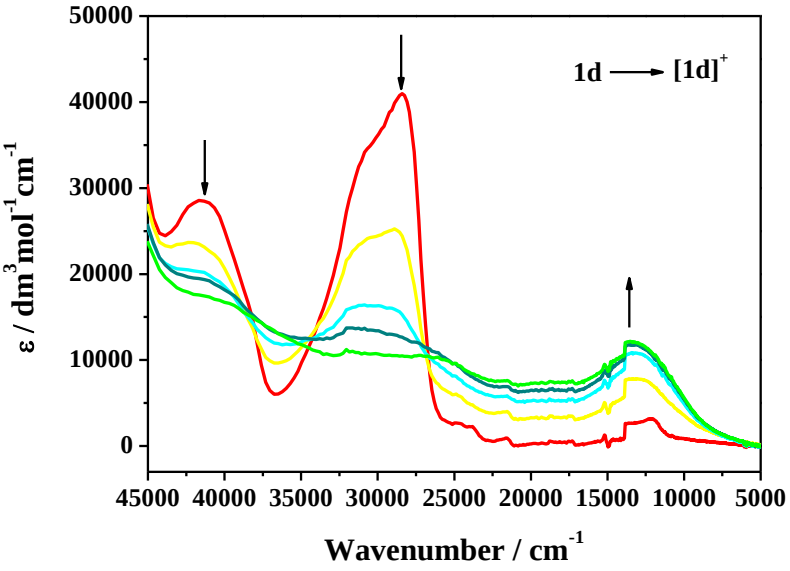

Figure S10. UV-vis-NIR spectral changes recorded during the oxidation of TMS-terminated reference compound **1d** to [**1d**]$^{+}$ in $CH_2Cl_2/10^{-1}$ M *n*-Bu_4NPF_6 at 298 K within an OTTLE cell.

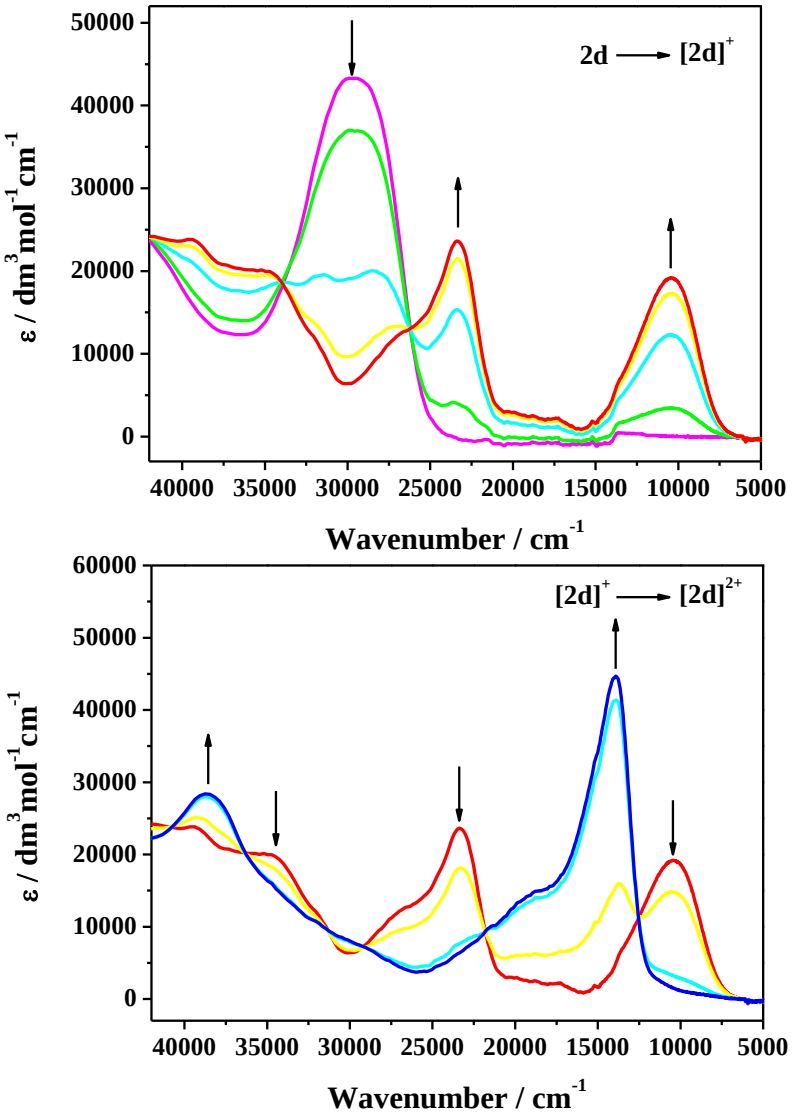

Figure S11. UV-vis-NIR spectral changes recorded during the oxidation of TMS-terminated reference compound **2d** to [**2d**]$^{+}$ (top), and [**2d**]$^{2+}$ (bottom) in $CH_2Cl_2/10^{-1}$ M *n*-Bu_4NPF_6 at 298 K within an OTTLE cell.

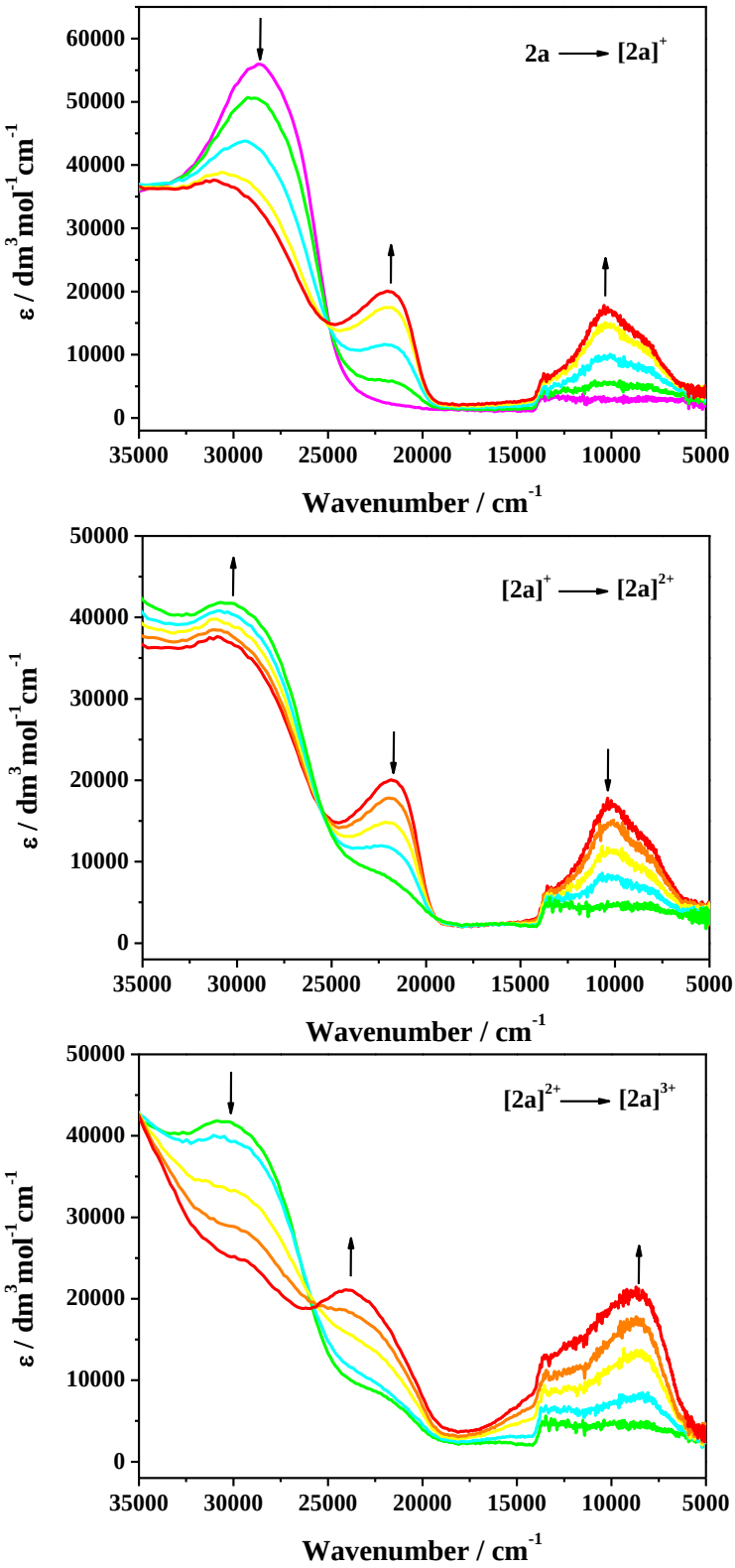

Figure S12. UV-vis-NIR spectral changes recorded during the careful stepwise oxidation of complex **2a** to [**2a**]$^{+}$ (top, not pure), [**2a**]$^{2+}$ (middle) and [**2a**]$^{3+}$ (bottom) in $CH_2Cl_2/10^{-1}$ M *n*-Bu_4NPF_6 at 298 K within an OTTLE cell. The generation of [**2a**]$^{+}$ is accompanied by some disproportionation to **2a** and [**2a**]$^{2+}$.

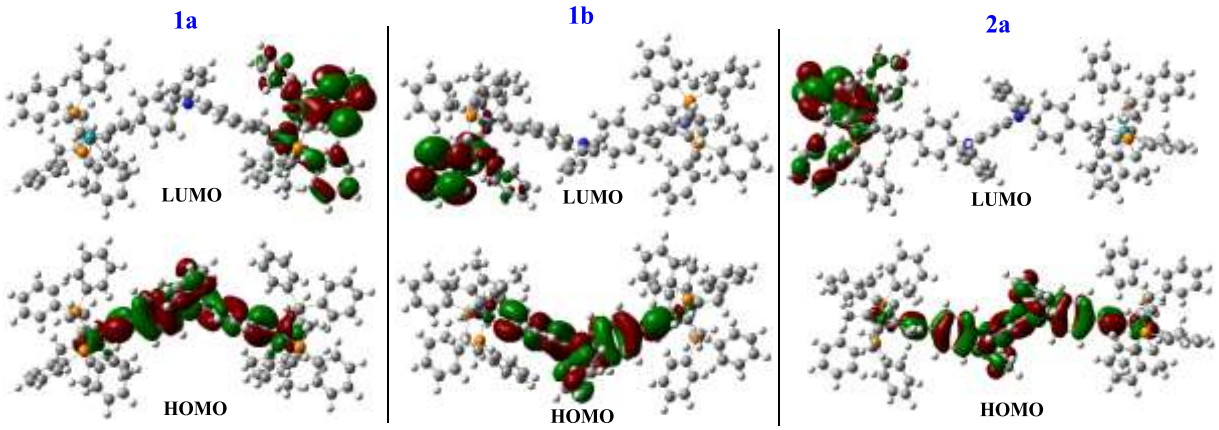

Figure S13. Frontier molecular orbitals of neutral complexes **1a**, **1b** and **2a** computed with the BLYP35/6-31G* method. Notably, the HOMOs are dominantly localized on the bridging ligands, which does not correspond with the asymmetric spin localization in the corresponding monocations, see Figure 6 in the main text.

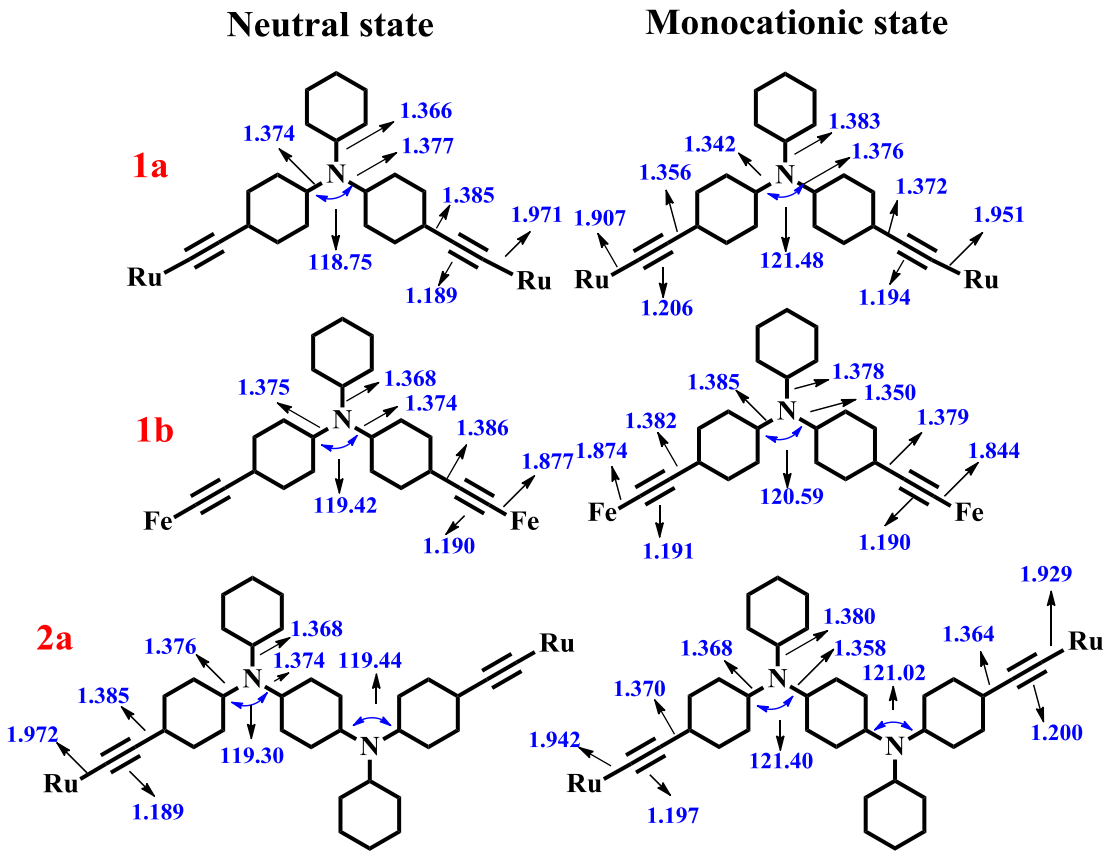

Figure S14. Schematic diagrams of structural parameters (bond length [Å] and angle [°]) in neutral (left) and mixed-valence monocationic (right) states of complexes **1a**, **1b** and **2a** resulting

from DFT calculations.

Table S2. Selected parameters derived from deconvolution of the NIR absorption band envelope in $[\mathbf{1a}]^{+}$.[a]

Complex	$[\mathbf{1a}]^{+}$
ν_1/cm^{-1} (ε_{max}/ dm^3 mol^{-1} cm^{-1})	10200 (18100)
ν_2/cm^{-1} (ε_{max}/ dm^3 mol^{-1} cm^{-1})	7800 (12400)
$\Delta(\nu_2)_{1/2}$[b]	2300
$\Delta(\nu_{IVCT})_{1/2}$(calc)[c]	4244
R_{ab}[d] (Å)	14.19
H_{ab} (cm^{-1})[e]	685

[a]The monocation was generated within a spectroelectrochemical cell from a solution in CH_2Cl_2/10^{-1} M *n*-Bu_4NPF_6. [b]The observed half-height bandwidth. [c]$\Delta(\nu_{IVCT})_{1/2}(calc) = 2[4\ ln(2)\nu_{IVCT}RT]^{1/2} = [2310\nu_{IVCT}]^{1/2}$ at ambient temperature. [d] Determined from the single crystal structure of **1a**. [e]$H_{ab} = (2.06\times10^{-2}/R_{ab})(\varepsilon_{max}\nu_{max}\Delta\nu)^{1/2}$.

NMR Spectra

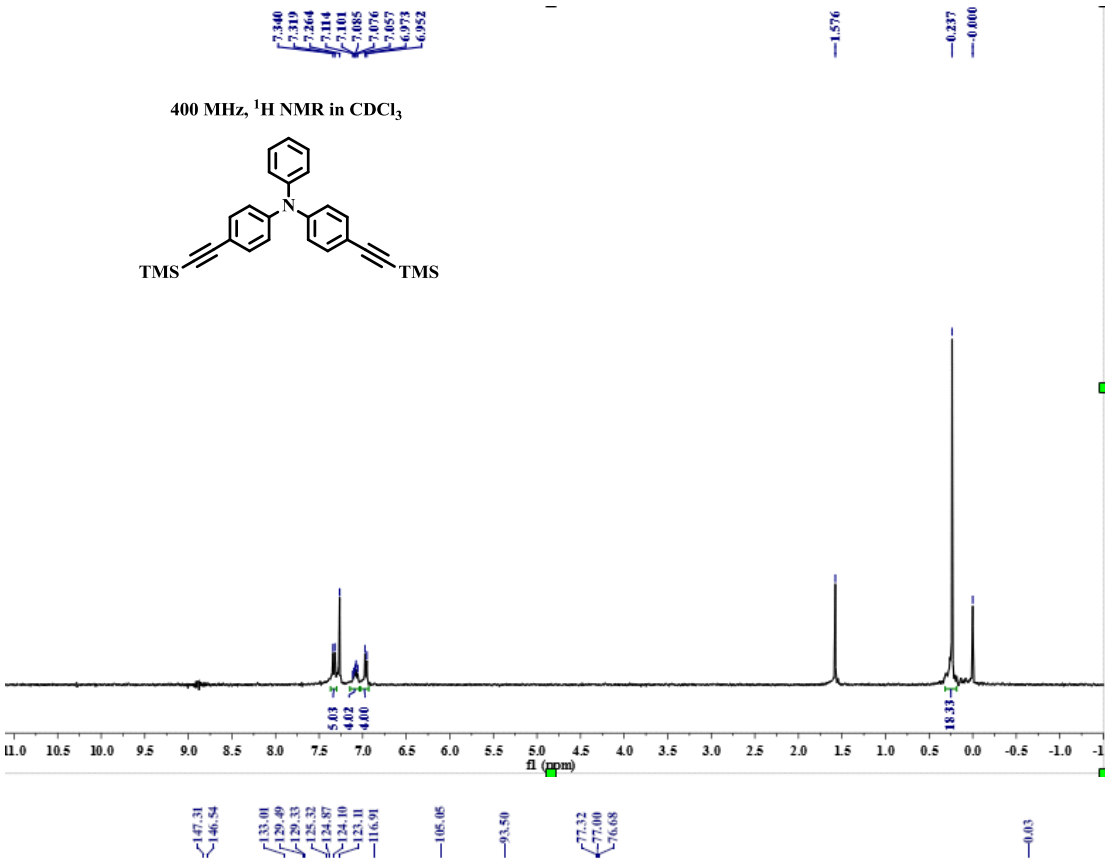

400 MHz, ^{1}H NMR in $CDCl_3$

100 MHz, ^{13}C NMR in $CDCl_3$

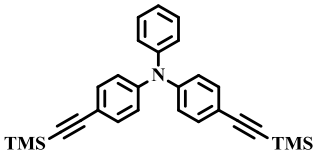

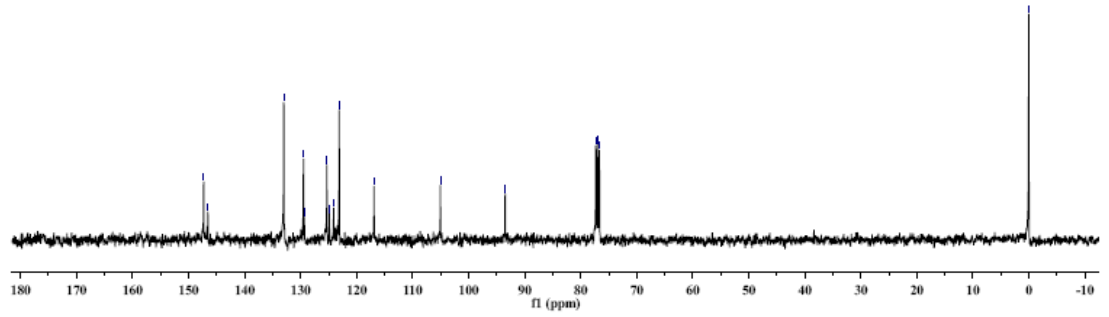


400 MHz, ^{1}H NMR in $CDCl_3$

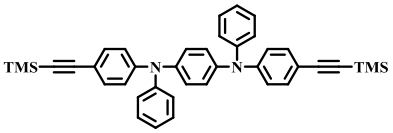

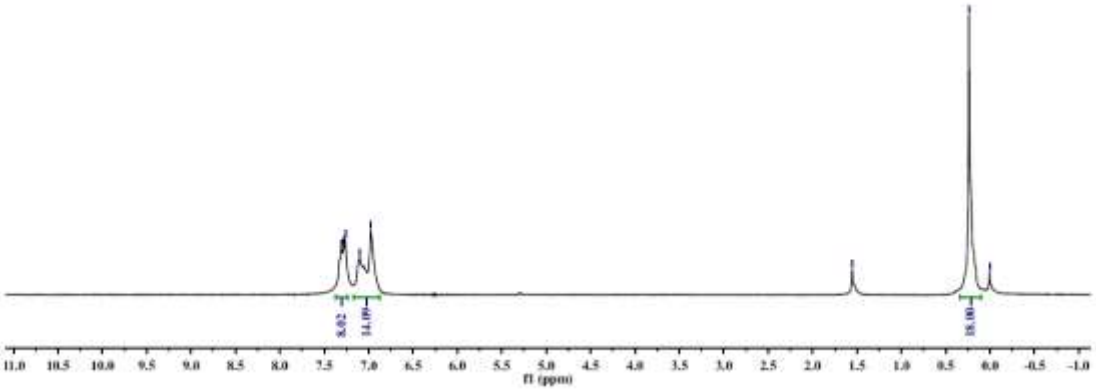

100 MHz, ^{13}C NMR in $CDCl_3$

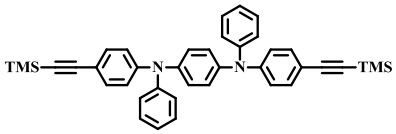

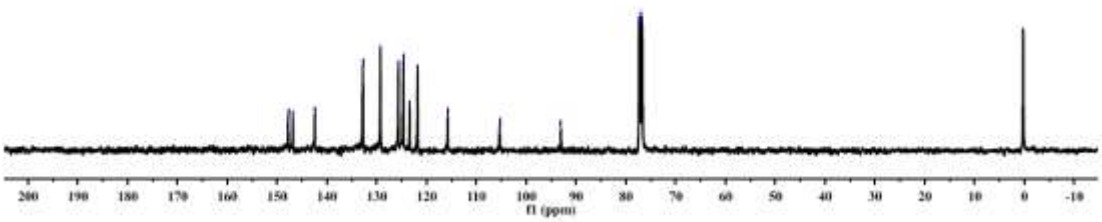

400 MHz, ^{1}H NMR in $CDCl_3$

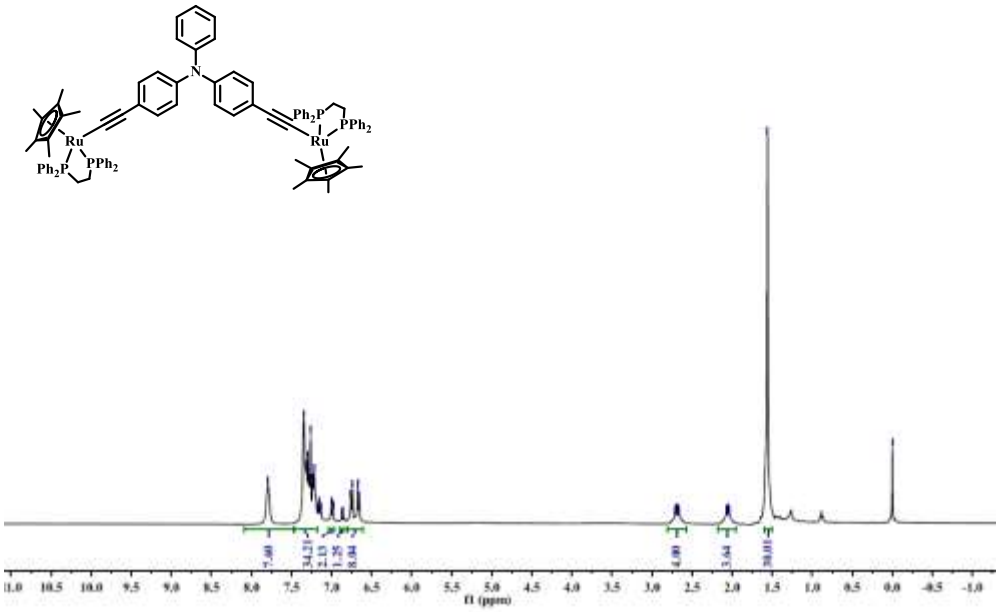

100 MHz, ^{13}C NMR in $CDCl_3$

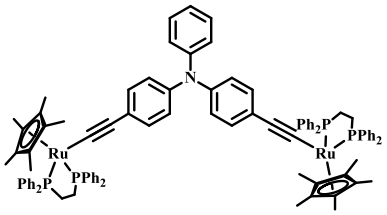

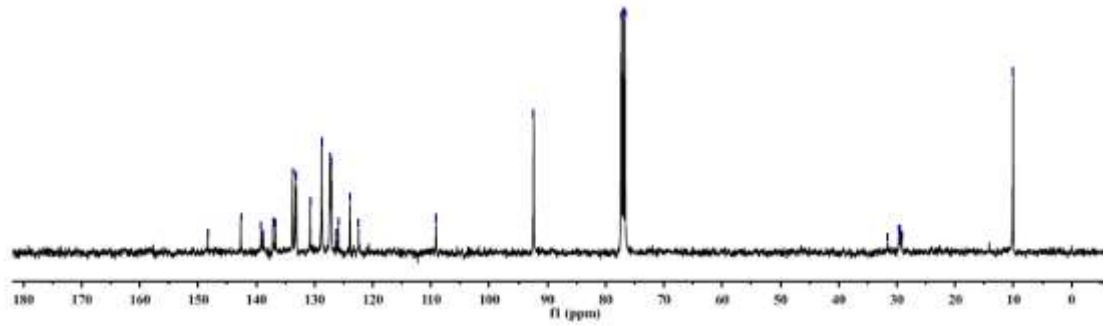

160 MHz, ^{31}P NMR in $CDCl_3$

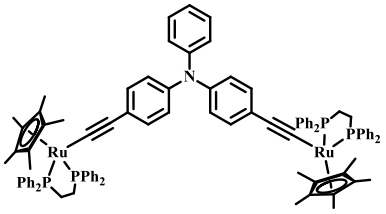

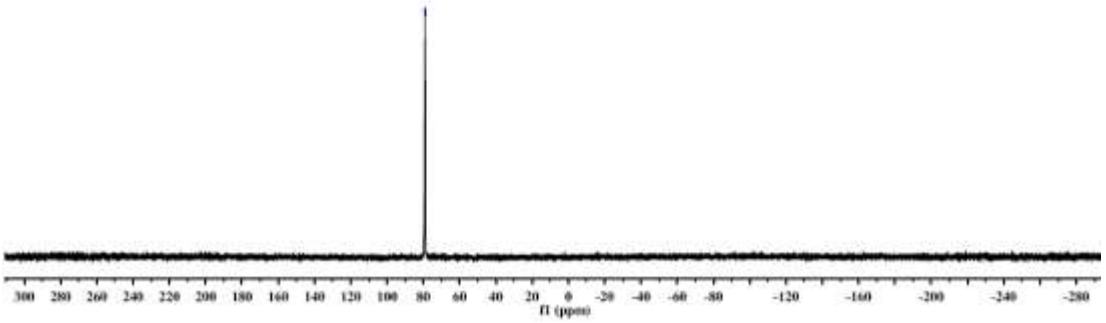

400 MHz, ^{1}H NMR in $CDCl_3$

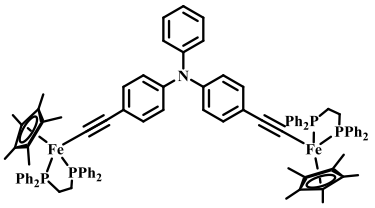

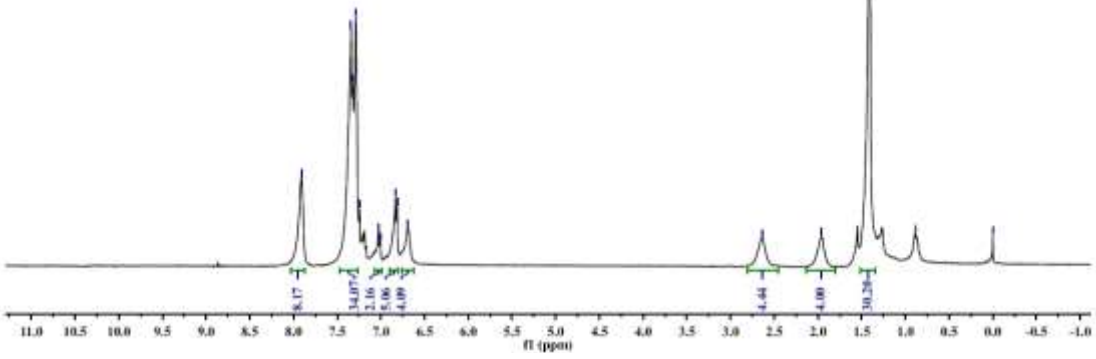

100 MHz, ^{13}C NMR in $CDCl_3$

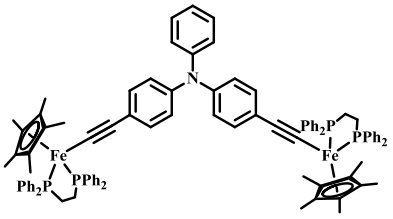

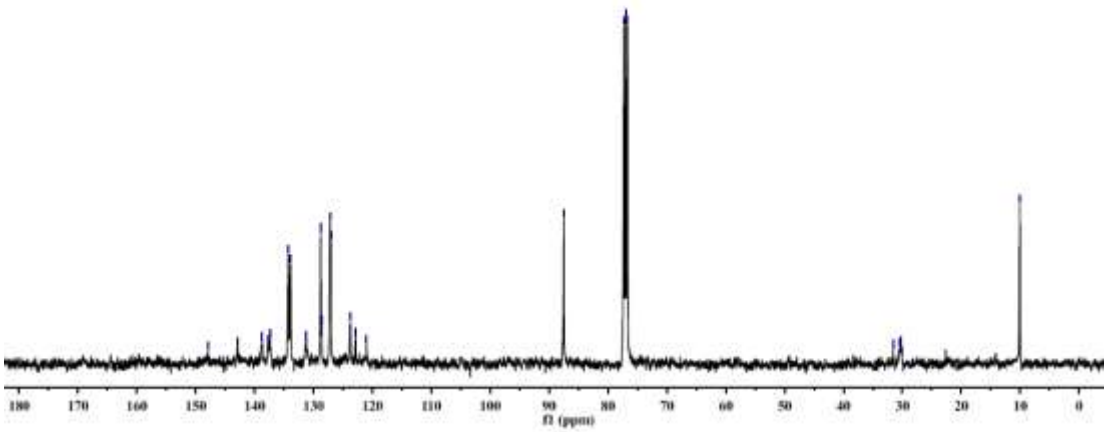

160 MHz, ^{31}P NMR in $CDCl_3$

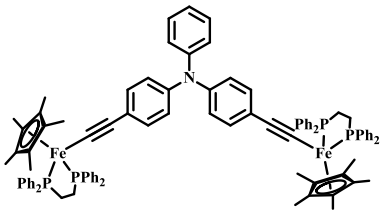

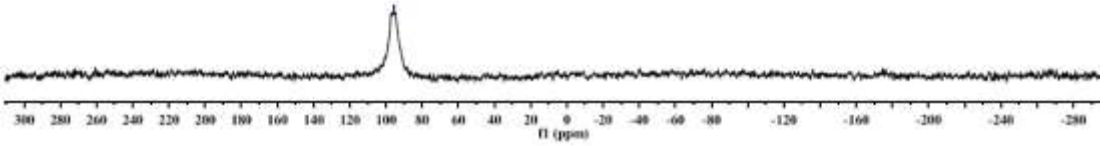

400 MHz, ^{1}H NMR in $CDCl_3$

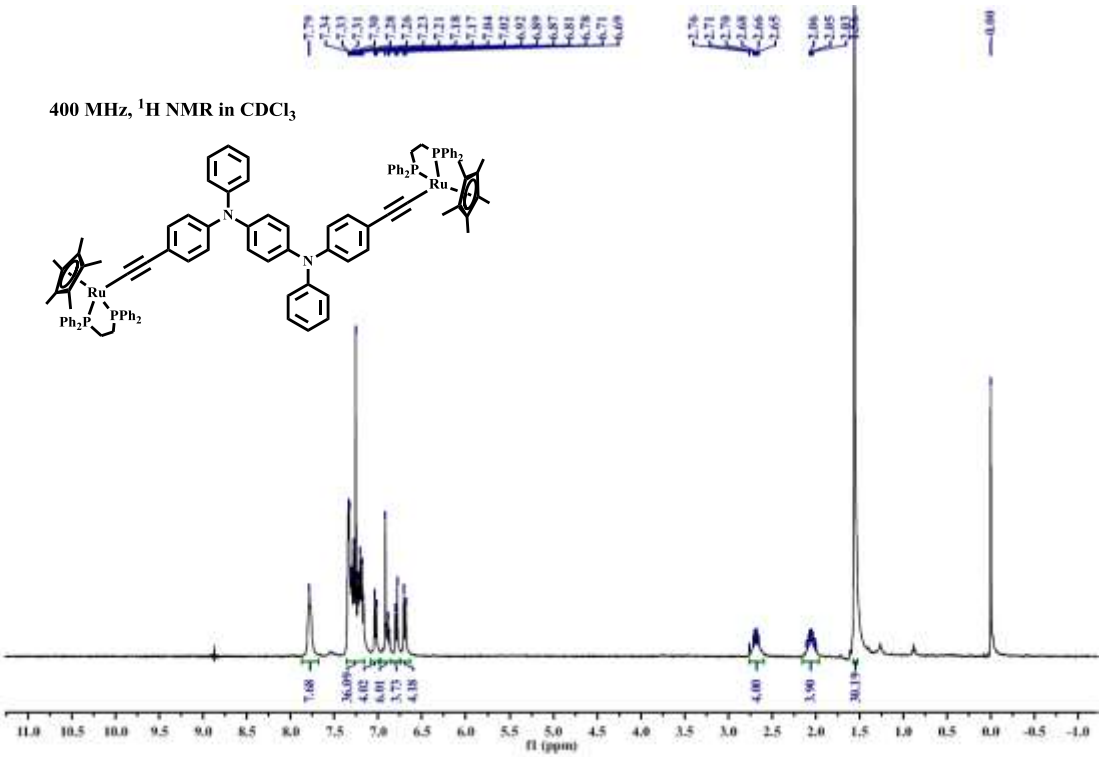

100 MHz, ^{13}C NMR in $CDCl_3$

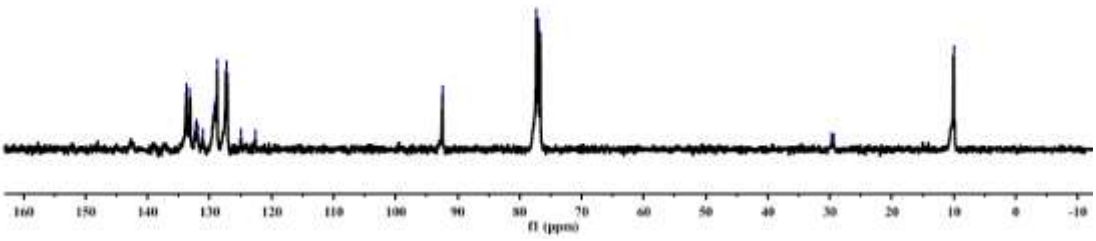

160 MHz, ^{31}P NMR in $CDCl_3$